

Predicting Radiation of CISPR 25 Complaint ALSE Environment

Jin Jia¹, Zhida Lai², Ruimiao Wang³, and Xu Li⁴

¹Chongqing University of Technology, Vehicle Engineering Institute, Chongqing, 401135, China

²State Key Laboratory of Vehicle NVH and Safety Technology, Chongqing, 401122, China

³State Grid Research Institute of Chongqing Electric Power Company, Chongqing 401123, China

⁴Chang'an Automotive Engineering Institute, Chongqing 401120, China

Abstract – According to the ALSE configuration in CISPR 25, cable bundle is often the dominant radiation structure due to the Common-Mode (CM) current. However this emission test method suffers from a need of a large anechoic chamber. In order to reduce this cost of electronic component development in the EMC test phase, this paper presents a CM current-scan to predict the radiated emissions from 30MHz - 1GHz; moreover, CM-voltage measurement on the cable bundle is also proposed from 150 kHz - 30 MHz. Both methods rely on simple radiating structures and do not take into account the complexity of a real ALSE environment. Therefore a calibration approach based on measured data is proposed to incorporate real influence factors in an anechoic shielded chamber. The proposed approaches are verified by different cable bundles and measurements.

Index Terms – ALSE method, cable bundle, CISPR 25, Common-Mode current, Common-Mode voltage, radiated emission.

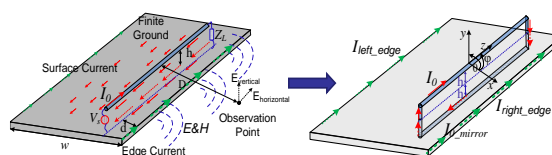
I. INTRODUCTION

Due to increasing clock frequencies and electronic modules, automotive cable bundles as primary interconnection medium enhance the complexity of electromagnetic behavior and the potential risk of functional safety. Electromagnetic emission evaluation (EME) for automotive electronic devices connected to cable bundle is necessary. For guaranteeing the reliability and reproducibility of the EME, common commercial electromagnetic compliance (EMC) limits specify test configuration and site. For example the ALSE method from CISPR 25 [1] specifies that radiated emissions measurements from electronic components or modules should be connected to a cable bundle of 1.5 m length. To eliminate extraneous disturbance and avoid wall reflections, it requires an anechoic shielded chamber characterized by high costs and space consumption. In order to reduce electronic-component development cost in EMC test phase, previous works [2]-[3] introduced current scanning method in frequency and time domain to substitute expensive anechoic chamber measurement

of ALSE method according to CISPR 25. One method is the current amplitude scanning method in frequency domain. The phase of CM current is retrieved from a specific optimization algorithm, only based on the measured amplitude of CM current. While the other method is current scanning method in time domain, which can obtain the amplitude and phase information of CM current simultaneously through Fast Fourier Transform (FFT). Both methods are based on a basic assumption that radiated emissions are mainly dominated by the CM current along the cable bundle. Consequently the CM current path can be modeled by a set of elementary dipoles and mirror current to evaluate radiated emissions from cable bundle. For solving the limitation of finite metallic ground in real test configuration, surface current model substituting mirror current is proposed in the final simulation calculation [4]. However, the prediction accuracy of alternative approaches is still confined by the real ALSE test environmental factor. Moreover previous current scan based method cannot solve the low-frequency due to the sensitiveness of phase measurement below 30 MHz [2]. Based on current scan methods in previous works, this paper focus more on measures to further improve radiation prediction accuracy. Besides, the CM voltage measurement is proposed to predict the radiated emissions at low frequencies.

II. RADIATION MODELS OF CISPR 25 CONFIGURATION

According to ALSE method in CISPR 25, the electronic component should be connected to 1.5 m wire or cable bundle to evaluate field emissions. Therefore this configuration mainly consists of a cable bundle and a finite metallic ground based on the assumption that CM current domains field emission, as shown in Fig. 1.



(a) Radiation from a cable bundle on a finite ground

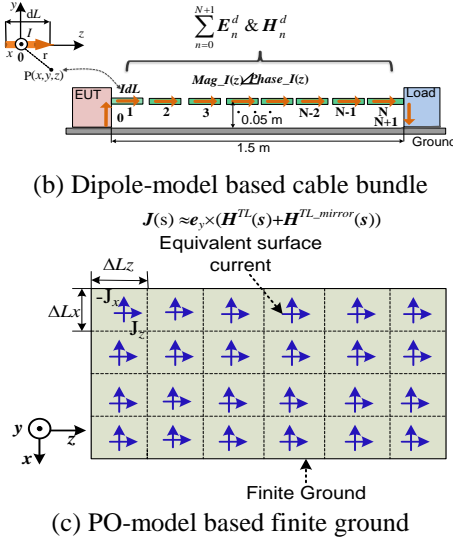


Fig.1. Radiation model from a cable bundle on a finite ground.

In Fig. 1, the radiation from the cable bundle is the sum of radiation from each dipole, according to [4]-[5]:

$$H_x(\omega) = \frac{-IdL \cdot y}{4\pi r} \beta_0^2 \left(j \frac{1}{\beta_0 r} + \frac{1}{\beta_0^2 r^2} \right) e^{-j\beta_0 r}, \quad (1)$$

$$E_y(\omega) = \frac{IdL \cdot zy}{4\pi r^2} \eta_0 \beta_0^2 \left(j \frac{1}{\beta_0 r} + \frac{3}{\beta_0^2 r^2} - j \frac{3}{\beta_0^3 r^3} \right) e^{-j\beta_0 r}, \quad (2)$$

where r is the distance from one dipole to the observation point P ; ϵ_0 is dielectric constant of vacuum; dL is Hertzian dipole length; I is the current on a dipole; η_0 is wave impedance in vacuum ($\eta_0 = \sqrt{\mu_0/\epsilon_0}$), where μ_0 is permeability of vacuum. β_0 is the electromagnetic wave phase constant in vacuum. While the finite metallic ground can be represented by an array of equivalent surface current, which also can be modeled by electric dipoles with physic optics (PO) method [6]. The radiation from this finite ground can be calculated according to (only y-component is shown):

$$E_y^P(\omega) = \sum_{k=1}^N \frac{I_{dipx}^k \Delta L_x^k \cdot zy}{4\pi r^2} \eta_0 \beta_0^2 \left(j \frac{1}{\beta_0 r} + \frac{3}{\beta_0^2 r^2} - j \frac{3}{\beta_0^3 r^3} \right) e^{-j\beta_0 r}, \quad (3)$$

where N is the mesh number of finite ground, r is the distance from a mesh center to observation point (x, y, z) , ΔL_x^k is the k^{th} mesh length along x -direction as shown in Fig. 1. Figure 2 shows the illustration of radiation calculation from typical ALSE method configuration. The total radiated field from the TL-finite ground plate system ($\mathbf{E}^{\text{Total}} \& \mathbf{H}^{\text{Total}}$) consists of two components; namely, the field due to TL in the absence of the plate ($\mathbf{E}^{\text{TL}} \& \mathbf{H}^{\text{TL}}$), and the field due to induced currents on the finite ground plate in the absence of the TL ($\mathbf{E}^{\text{P}} \& \mathbf{H}^{\text{P}}$). In the process diagram, $\mathbf{H}(s)$ is tangential magnetic on surface of finite ground plate and $\mathbf{J}(s)$ is equivalent surface current density on it. While (x, y, z) is Cartesian

coordinate of field observation point.

To verify the multi-dipole model for the cable bundle and surface current model for the finite ground plate [7]-[9], electric fields at the observation point in Fig. 1 are calculated by the proposed model and MoM, as shown in Fig. 3. It can be seen that the simulated electric field from proposed models matches very well with the result from MoM. Besides the field at the observation point with 1 m distance, the far field radiation pattern ($0^\circ \leq \theta \leq 180^\circ$) on the plane $\phi = 0^\circ$ with 10 m distance are also investigated, which refers to the spherical coordination system in Fig. 4 (up). Figure 4 (down) also shows the good matching of radiation pattern at 300 MHz, which are calculated by MoM and surface current model respectively.

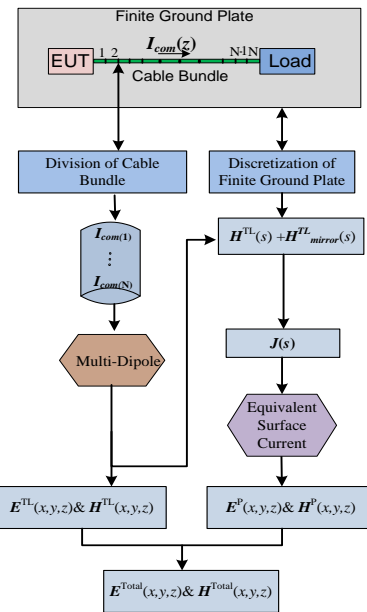


Fig. 2. Illustration of radiation models from cable bundle based on the multi-dipole model and the finite ground based on the surface current model.

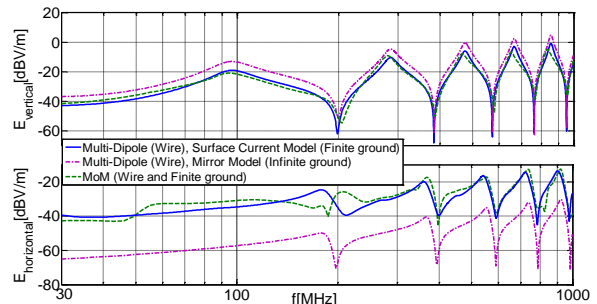


Fig. 3. Comparison of electric field in vertical (upper) and horizontal (lower) polarization at observation point between surface current model and MoM model.

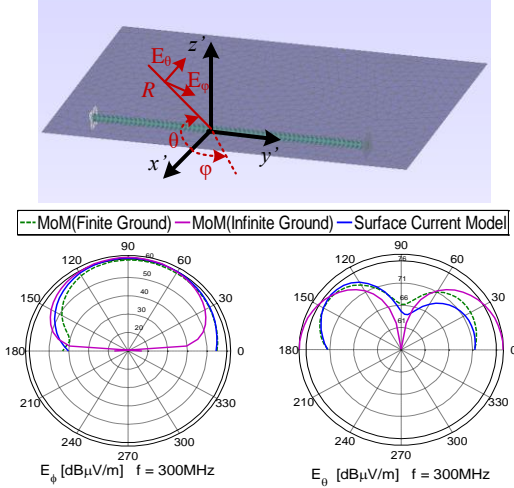


Fig. 4. Radiation pattern from the MoM and the surface current model on the plane $\phi=0^\circ$ at 300.

III. IMPROVING ACCURACY OF RADIATION PREDICTION WITH CORRECTION FUNCTION

According to CISPR 25, the ALSE test method must be implemented in an anechoic shielded chamber with a specific test antenna. From 150 kHz to 30 MHz, an active Rod antenna (SCHWARZBECK VAMP 9243 in this work) can be used to measure the vertical electric coupling field; from 30 MHz up to 1 GHz a Bilog antenna (TESEQ CBL 6141B in this work) can be used to measure both the vertical and horizontal electric field, as shown in Fig. 5. The proposed simplified and ideal radiation models are problematic due to the complex behavior of the anechoic chamber, where peripheral systems and reflections from the chamber walls can influence the antenna voltage. Thereby it is necessary to take these factors into account. For this purpose a measurements based calibration procedure is proposed.

A 1.5 m long single wire, fed by a sinusoidal signal, is used. Then corresponding correction function for the ALSE environment can be obtained:

$$K_C = E_{sim} - E_{antenna} \quad (dB) \quad (4)$$

$$E_{antenna} = V_{antenna} + AF_{antenna} \quad (dB)$$

Here $E_{antenna}$ is the measured electric field, which is the sum of antenna voltage $V_{antenna}$ and the specific antenna factor $AF_{antenna}$. It involves the influencing factors from ALSE environment. E_{sim} is the simulated field at the antenna reference point based on the scanned current data from the measurement configuration model. It involves errors from current data and radiation models. For high accuracy, the measurement equipment and all the coaxial cables in process of current scanning should be maintained similar as in the process of antenna measurement. These correction functions are the fingerprint of a test chamber and will vary from location

to location. Therefore calibration procedure needs to be applied in each test chamber to obtain their respective correction functions. This procedure can also be a very useful method to compare different test chambers.

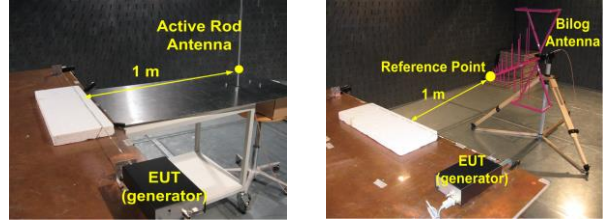


Fig. 5. ALSE test configurations for the active Rod antenna (left) and the Bilog antenna (right).

A. Calibration by an active Rod antenna below 30 MHz

In the active Rod antenna set-up as shown in Fig. 5 (left), the active impedance convertor should give a frequency independent coupling factor, due to the high input impedance. However, taking into account the capacitive coupling between metallic table and chamber floor, as well as the inductive coupling from connected coaxial cable to antenna, this coupling factor is no longer a straight line [10]. For example in Fig. 6, a rise occurs above 2 MHz in the ALSE test configuration, depicted by measurement curve labeled by *ALSE*. When the calibrated wire and active Rod antenna are placed on the chamber floor to remove the capacitive table coupling, this rise cannot be observed anymore as denoted by the measurement curve labeled by *Chamber-Floor*. Some measures could suppress the coupling effects in the ALSE configuration to guarantee the test accuracy, for example adjusting the antenna height or counterpoise grounding. The correction function K_C , which describes the deviation between antenna measurement and simulation from 2 MHz to 30MHz, is about 7 dB. Here the simulation is based on multi-dipole model for the wire and mirror model for the ground plate. K_C can be used as a correction function to compensate the error due to capacitive table coupling.

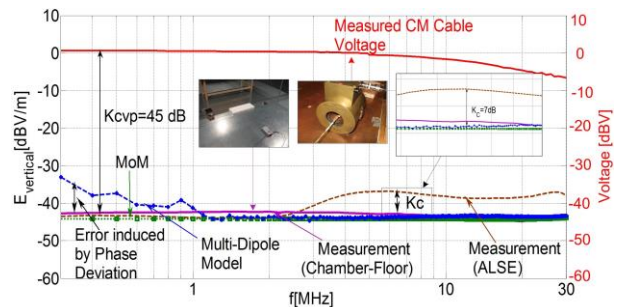


Fig. 6. Normalized measured and simulated data from the calibration of active Rod antenna.

In order to fix low-frequency problem using current scan method, directly measured cable voltage by a Common-mode Voltage Probe (CVP) [11] with known coupling function K_{CVP} can be used as alternative to evaluate radiated field at very low frequencies. The function K_{CVP} between the measured cable voltage and the measured electric field of active Rod antenna is about 45 dB below 5 MHz, and it can be defined by:

$$K_{CVP} = V_{Cable} - E_{Rod-antenna} \text{ (dB)} \quad (5)$$

$$E_{Rod-antenna} = V_{Rod-antenna} + AF_{Rod-antenna} \text{ (dB)}$$

This coupling function should be constant at low frequencies, but it will vary with different CVPs, active Rod antennas or test sit

B. Calibration by a Bilog antenna from 30 MHz to 1 GHz

In the analysis of active Rod antenna below 30 MHz, the mirror currents and multi-dipole radiation model in simulations are accurate enough to model the metallic table in Fig. 5 (left). However for the Bilog antenna used from 30 MHz to 1 GHz, an infinite ground model and mirror theory cannot reflect the influence of the finite metallic plate, especially in horizontal polarization. Therefore, the more accurate surface current model is used. To calculate the correction function with (4), the wire current distribution measurement and antenna measurement are both required. Figure 7 is the configuration to acquire current amplitude distribution on the single wire in the frequency domain. Current acquired in time domain is similar to this configuration, but an extra reference probe is needed.

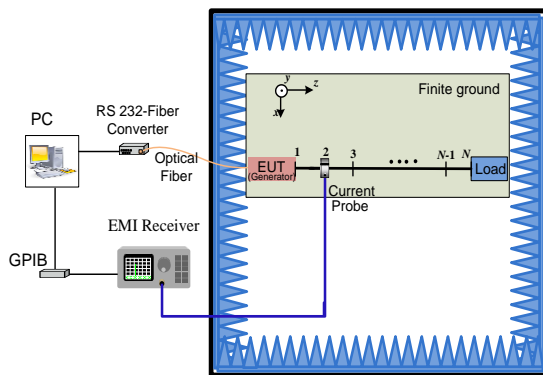


Fig. 7. Calibration configuration for the current scan method in frequency domain.

In the calibration of the Bilog antenna using frequency-domain current scan method, the wire current amplitude distribution is measured by an EMI receiver and the phase distribution is retrieved by proposed retrieval algorithm. Then they are applied to calculate electric fields at reference point depicted in Fig. 5 (right), based on multi-dipole radiation model for the wire and

surface current model for the finite ground plate. Figure 8 shows the vertical electric field from direct antenna measurements, proposed simulation methods, and MoM. K_C denoted in plot is the correction function according to Equation (4), representing the deviation between the simulated field based on scanned current and the measured field directly from Bilog antenna. Also horizontal field at reference point is calculated as shown in Fig. 9. Compared with the vertical component, the horizontal component in measurement is more sensitive to the configuration, especially at high frequencies.

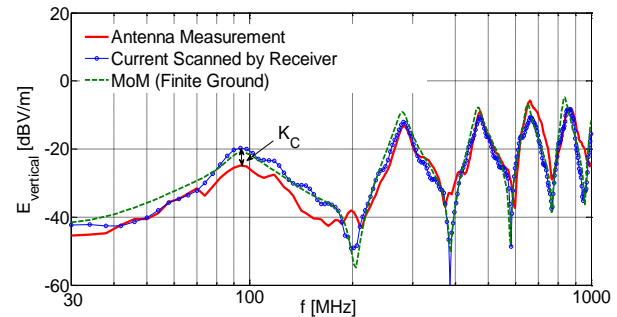


Fig. 8. Measured and simulated vertical field from the calibration configuration based on the scanned current by the EMI receiver.

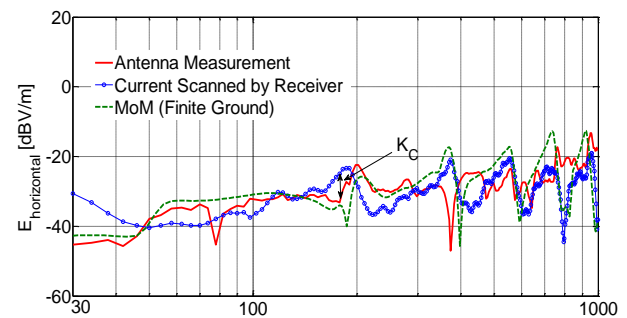


Fig. 9. Measured and simulated horizontal field from the calibration configuration based on the scanned current by the EMI receiver.

Likewise, calibration of the Bilog antenna using time-domain current scan method is implemented with the same procedure. But current amplitude and phase along the calibrated wire are both acquired from an oscilloscope and FFT transformation.

C. Load dependence of correction functions

In the calibration procedure shown above, the single wire is terminated by a 50Ω load. Correction function is nearly a constant with different loads in the active Rod antenna calibration. However, in the Bilog antenna calibration the correction function varies with different loads over frequency resonance minimums. Therefore,

different loads terminated at the calibrated wire can obtain a set of correction functions. The average of these correction functions is more reasonable, because the common-mode current on a real cable bundle would encounter complex terminal circumstances at different frequencies. Figure 10 present the correction functions with short, open, 1 kΩ loads and their average data in the vertical polarization, respectively. It can be observed that an apparent difference in correction functions due to different loads occurs around 200 MHz, 400 MHz, 600 MHz, 800 MHz and 1000 MHz in vertical polarization, which are also around resonance minimums in vertical electric field curve as shown in Fig. 8. With the same procedure average correction function also can be obtained in the horizontal direction.

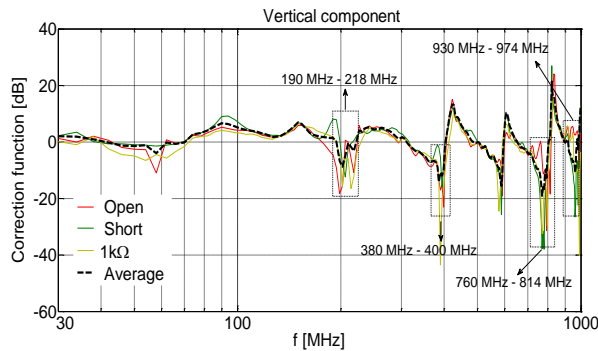


Fig. 10. Correction functions in the vertical polarization.

IV. RESULTS AND EXPERIMENTS

In order to verify the proposed simulation methods considering real ALSE environments, a cable bundle with seven wires is used. Moreover, a real stepper-motor systems is also built to verify proposed methods and improvements.

A. Cable bundle with seven wires

Figure 11 shows the test configuration according to ALSE method. Fed cable is driven by a 3.3 V digital signal with 40 MHz, of which rising time and falling time are about 2.5 ns. Source wire is terminated by a 50 Ω load, and other wires are terminated resistors. In the antenna measurement the reference point of Bilog antenna is 1 m distant to the cable bundle center. The antenna voltage is measured by the EMI receiver (average detector, 120 kHz BW, and 5 ms MT). In the current scan methods, the CM currents on the cable bundle are acquired by the EMI receiver with same setting as the antenna measurement, or acquired by the oscilloscope (single sweep, 550 μs sample time, and 0.5 ns interval time). Multi-dipole radiation model for the cable bundle and surface current model for the finite ground are applied to predict the radiated field at the reference point of Bilog antenna. After correcting these predicted results using the available correction function, the comparisons between the direct

antenna measurement and the simulation are depicted in Fig. 12 (only vertical polarization is shown here).

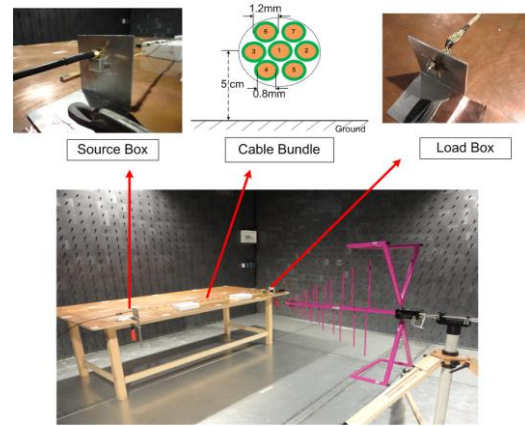


Fig. 11. Configuration with seven-wire cable bundle.

Figure 13 depicts the deviation bar charts compared with the antenna measurement. Twelve main harmonics (integral multiples of the fundamental-frequency 40 MHz) are shown. In vertical polarization, most deviations from the current measured by the EMI receiver are below 4 dB. Deviations from the current measured by the oscilloscope can be less than 5 dB except at 360 MHz. Compared with vertical fields, the calculated horizontal fields show higher deviation. Maximum deviation from simulation nearly amounts to 13 dB at 280MHz and 480 MHz. The proposed averaged correction functions from the calibration procedure can improve the predicted accuracy of current scan methods. For example, the simulation results including correction functions can improve the accuracy by 1.5 dB ~ 11 dB in the vertical field and 3 dB ~ 13 dB in the horizontal field at main radiation peaks, as shown in Fig. 14. However, the accuracy of horizontal field at 280 MHz is reduced after adding an unreliable value of 8.3 dB. This frequency is close to 300 MHz, where the correction function is very sensitive to load impedances.

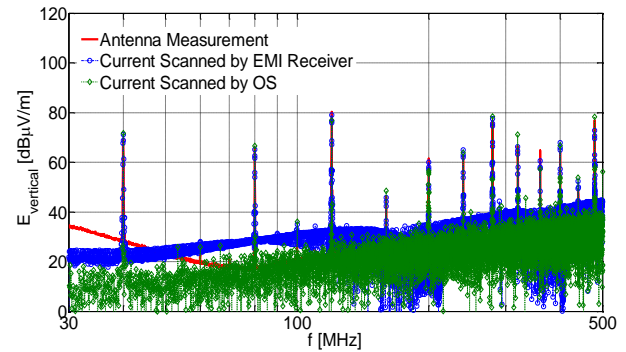


Fig. 12. Vertical electric field from the antenna measurement and the simulation based on the cable current scanned by EMI receiver and oscilloscope (OS).

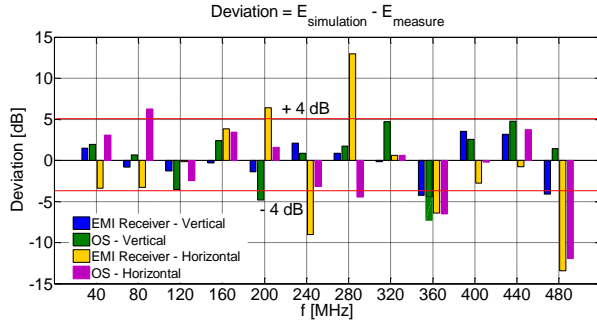


Fig. 13. Deviations of calculated fields based on the cable current scanned by the EMI receiver and the oscilloscope (OS) compared with antenna measurement.

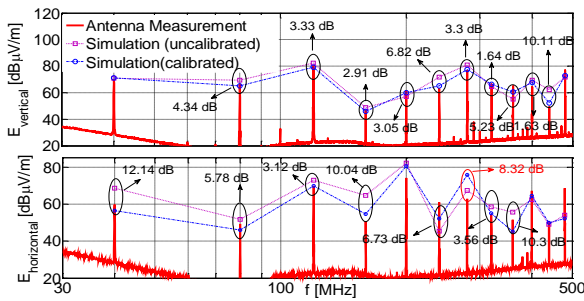


Fig. 14. Electric fields from antenna measurement and simulation based on the cable current scanned by the EMI receiver with and without correction functions.

B. Stepper-motor drive system

Figure 15 shows the radiation test configuration with the Bilog antenna (30 MHz to 1 GHz) and the active Rod antenna below 30 MHz. For flexibility in programming, a microcontroller board (Arduino with 16 MHz-clock frequency) with a motor drive board is applied as EUT, which is similar to typical automotive electronic control units. A 20 dB pre-amplifier (Rohde&Schwarz Hz-16) is used to improve the measurement dynamics.

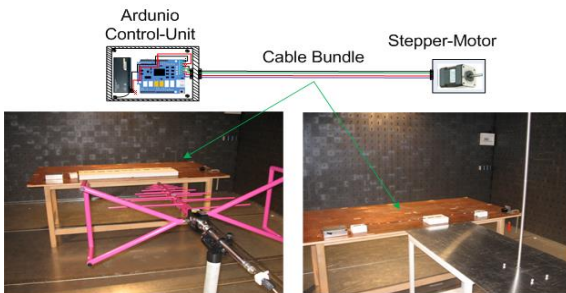


Fig. 15. Analyzed configuration of a stepper-motor drive system.

EMI receiver (average detector, 120 kHz BW, and 5 ms MT) is used to measure the antenna voltage, and the

voltage can be transferred to electric field at the antenna reference point with the antenna factor. Electric fields at the reference point are also calculated based on the acquired cable current by the EMI receiver with same setting as antenna measurement, or by the oscilloscope (single sweep, 550 μs sample time, and 0.5 ns interval time). Figure 16 shows the main radiation peaks of vertical or horizontal fields, which exceed the average limits according to CISPR 25. Some of these peaks might disturb the commercial frequency band, for example the peak at 96 MHz is located in FM band and it exceeds the class-2 limit. In addition, the CM current distributions with respect to these peaks are also depicted. They flow along the cable bundle in the form of current standing wave. From these curves, a current distribution in the order of several decibels in μA also may exceed the radiation limit, for example the maximal value of current distribution at 384 MHz is less than about 10 dBμA.

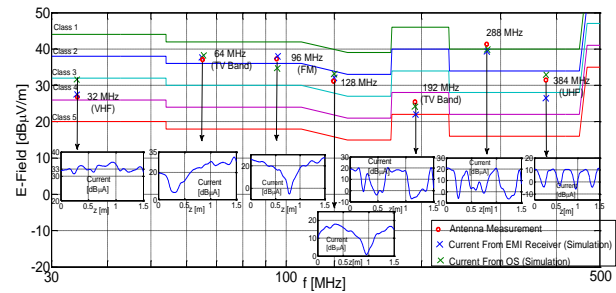


Fig. 16. Average limits for radiated disturbs from CISPR 25 and main radiation peaks from stepper motor drive system associated with the corresponding common-mode current distributions.

As well as the prediction of radiated emissions above 30 MHz, radiated emissions from the stepper-motor drive system at low frequencies are also investigated. Figure 16 (right) shows the active Rod antenna test set-up according to the ALSE method. Due to the difficulty of the proposed frequency-domain scan method to predict the field emission at low frequencies, only time-domain scan method is applied here. Capacitive coupling from the metallic table to the chamber ground can be corrected by K_C denoted in Fig. 17. Calculated results from time-domain scan method and antenna measurement are both depicted in Fig. 6. It can be seen that simulation has high accuracy at the clock frequency of 16 MHz and the first harmonic of 32 MHz, where the error is less than 2 dB. However, the results still have a large deviation below 5 MHz, due to the high sensitivity of the multipole radiation model to phase distribution error. Moreover, the noise from the pre-amplifier during current acquisition at low frequencies is also an important factor in degradation of the prediction accuracy. In order to solve this problem at very low frequencies, the cable

voltage measurement by the CVP with correction function K_{CVP} is another alternative as shown in Fig. 6. Figure 18 depicts the vertical field from direct antenna measurement and the cable voltage minus K_{CVP} in decibel. Compared with cable-current based alternative, the cable-voltage based method can obtain better prediction accuracy with higher reliability especially below 5 MHz.

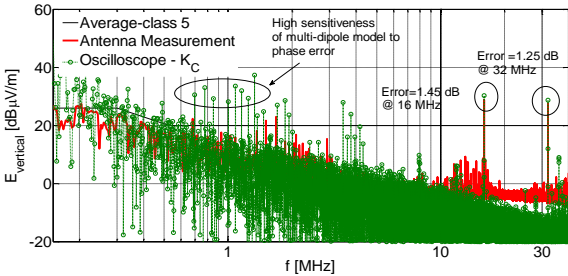


Fig. 17. Vertical electric fields from the stepper-motor drive system by the antenna measurement and the simulation based on the cable current scanned by the oscilloscope.

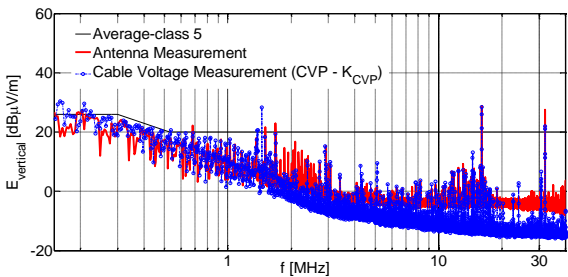


Fig. 18. Vertical electric fields from the stepper-motor drive system by the antenna measurement and the cable voltage measurement.

V. CONCLUSION

This paper proposed some measures to improve the accuracy of radiation prediction, which is based on current scan methods and typical ALSE radiation models in previous works. After acquiring current on the cable bundles, the electromagnetic fields can be calculated quickly by a multi-dipole model and surface current model. Real ALSE measurement environment influences need to be integrated in the simulation models for the comparison to the direct antenna measurements. Therefore, In order to reduce the deviations a calibration procedure was introduced to improve the prediction quality. In the calibration procedure, average correction functions was used considering different load impedance in real test scenarios. Moreover, a CM voltage alternative was proposed to predict radiation, which can overcome the low-frequency problem when using current scan methods. For validation of the methods, different configurations were analyzed. Radiated emissions from

a seven-wire cable was analyzed. Furthermore, a 4-wire bundle terminated with a stepper-motor and a micro-controller based motor driver were investigated. It could be shown that the proposed measures can improve prediction accuracy effectively considering the real ALSE configuration.

ACKNOWLEDGMENT

This work was supported in part by the project of Research on EMI mechanism and On-load test method of motor controller in the Electrical Vehicles (Nr. cstc2018jcyjAX0621), and part by the 2019 open fund from State Key Laboratory of Vehicle NVH and Safety Technology (Nr. NVHSL-201914).

REFERENCES

- [1] CISPR 25 Ed.3, "Vehicles, boats and internal combustion engines-Radio disturbance characteristics – Limits and methods of measurements for the protection of on-board receivers," 2007.
- [2] J. Jia, D. Rinas, and S. Frei, "Prediction of radiated fields from cable bundles based on current distribution measurements," *EMC Europe 2012*, Rome, pp. 1-7, Sept. 2012.
- [3] J. Jia, D. Rinas, and S. Frei, "Predicting radiated emissions of automotive systems according to CISPR 25 using current scan methods," *IEEE Trans. Electromagn. Compat.*, vol. 58, no. 2, pp. 409-418, 2016.
- [4] C. Paul and S. Nasar, *Introduction to Electromagnetic Field*. 2nd ed., McGraw-Hill, New York, 1987.
- [5] D. Schneider, M. Beltle, B. Siegel, S. Tenbohlen, and W. Kohler, "Radiated emissions of an electric drive system estimated on a bench using disturbance currents and transfer functions," *IEEE Trans. Electromagn. Compat.*, vol. 57, no. 3, pp. 311-321, Mar. 2015.
- [6] V. Volski and G. A. E. Vandenbosch, "Efficient physical optics approximation for the calculation of radiation pattern of planar antennas located on a finite ground plane," *IEEE Trans. Electromagn. Compat.*, vol. 53, no. 1, pp. 460-465, Jan. 2005.
- [7] J. Jia, F. Kremer, and S. Frei, "Modellierung von CISPR-25 antennenmessungen mittels schneller approximierender berechnungsverfahren," *EMV-Düsseldorf*, Germany, 2012.
- [8] J. Meng, Y. X. Teo, D. W. P. Thomas, and C. Christopoulos, "Fast prediction of transmission line radiated emissions using the Hertzian dipole method and line-end discontinuity models," *IEEE Trans. Electromagn. Compat.*, vol. PP, no. 99, pp. 1-9, May 2014.
- [9] Y. Vives-Gilbert, C. Arcambel, A. Louis, F. De Daran, P. Eudeline, and B. Mazari, "Modeling magnetic radiation of electronic circuits using near-

- field scanning method,” *IEEE Trans. Electromagn. Compat.*, vol. 49, no. 2, pp. 391-400, May 2007.
- [10] C. W. Fanning, “Improving monopole radiation emission measurement accuracy; RF chamber influences, antenna height and counterpoise grounding (CISPR 25 & MIL-STD-461E vs MIL-STD-461E),” *IEEE International Symposium on EMC*, Chicago, pp. 103-109, Aug. 2009.
- [11] S. Frei, T. Nägel, and R. Jobava, “Bestimmung der störaussendung im KFZ durch die getrennte betrachtung der elektrischen und magnetischen verkopplungen,” *EMV-Düsseldorf*, Germany, 2004.



Jin Jia received his Ph.D. degree in Electrical Engineering from the TU Dortmund University, Germany, in 2015. From 2015 to 2018 he worked as EMC engineer in China Automotive Engineering Research Institute (CAERI), Chongqing, China. Now he works in Chongqing University of Technology as a Senior Engineer. His main research interests include radiation modeling of complex cable bundles and EMC modeling of automotive electrical and electronic systems in electric and intelligent vehicles.